International Journal of Modern Physics A
Vol. 35, Nos. 34 & 35 (2020) 2044007 (10 pages)

DOI: 10.1142/S0217751X20440078

The ATLAS electron and photon trigger performance in Run 2

Daniela Maria Köck
on behalf of the ATLAS Collaboration
School of Mathematical and Physical Sciences,
Pevensey II, University of Sussex, Brighton, BN19QH, UK
daniela.maria.koeck@cern.ch

Received 5 February 2020
Accepted 6 November 2020
Published 18 December 2020

Electron and photon triggers are an important part of many physics analyses at the ATLAS experiment, where electron and photon final states are considered. Understanding the performance of electron and photon triggers at the High Level trigger as well as the Level-1 trigger was crucial to improve and adapt the trigger during changing run conditions of the Large Hadron Collider in Run 2 (2015–2018).

Keywords: ATLAS; Run 2; trigger; electron; photon; performance.

PACS number: 29.90.+r

1. Introduction

The High Level trigger system of the ATLAS experiment[1] at the CERN Large Hadron Collider is filtering proton–proton (heavy-ion) collisions happening up to every 25 (75) ns.[2] Electrons and photons are a distinctively clean signature in the ATLAS detector, both leaving their energy in the electromagnetic calorimeter, presenting an interesting signature for many beyond the standard model searches as well as precision measurements. Understanding the performance and efficiency of both electron and photon triggers is an important prerequisite to any analysis. These proceedings will provide a summary of the electron and photon trigger performance during the Run 2 collisions recorded by the ATLAS experiment from 2015 to 2018. For a more extensive discussion, please refer to Ref. 3.

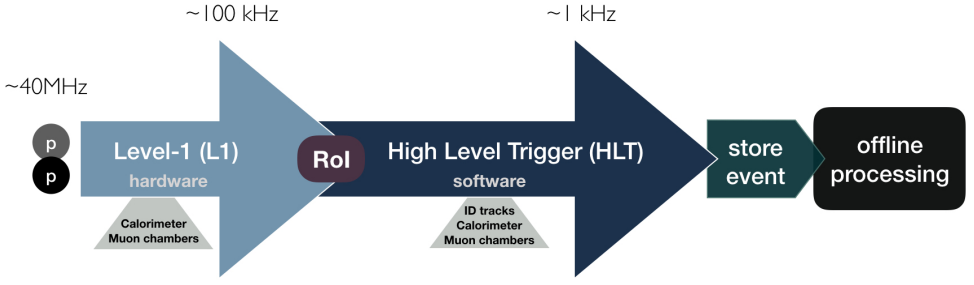

Fig. 1. The ATLAS trigger system illustrated on its main components, the Level-1 hardware trigger, as well as the High Level trigger in software. The given rates are the bunch-crossing rate, the L1 acceptance rate as well as the maximum HLT acceptance rate for proton–proton collisions.

2. The ATLAS Trigger System in a Nutshell

The ATLAS trigger system has a two-level structure, as illustrated in Fig. 1. A first selection is hardware-based, using information from the hadronic and electromagnetic calorimeters as well as the muon spectrometer. This step is known as the Level-1 (L1) trigger, which reduces the proton–proton collision rate from up to 40 MHz down to about 100 kHz.[3]

A Region-of-Interest is defined and passed on from the L1 trigger towards the High Level trigger (HLT), which is software-based and can use information from the calorimeters, the muon system as well as Inner Detector tracking information. Once a collision event has been selected by the HLT (with a rate of around 1 kHz), the event is stored. Every processing that happens after an event has been stored by the trigger is referred to as "offline processing."

At the HLT processing, several algorithms run consecutively, based on the information passed on from the L1 trigger. Each algorithm performs a selection of events, increasing in precision from a set of fast reconstruction steps to a precision reconstruction step, which is close to the offline reconstruction. These consecutive steps can be seen in Fig. 2(a), which details the electron trigger reconstruction sequence. For the use of triggers in analyses, all the main criteria put in the reconstruction sequence are decoded in the name of a trigger (see Fig. 2(b)). This includes the type of particle triggered on with its energy threshold, the identification criteria that is required for this particle, optional isolation criteria as well as the L1 threshold. At L1 the energy threshold can be extended with an η-dependent variation of this threshold (**V**), a veto against leakage of energy deposits into the hadronic calorimeter (**H**) as well as an isolation of the electromagnetic energy clusters (**I**).

The electron and photon triggers and trigger algorithms have undergone several changes within Run 2. One of the most significant changes for electrons has been the replacement of the "Fast Calorimeter Reconstruction" and "Efficient Selection" algorithm steps with a Neural-Network-based algorithm called Ringer in 2017

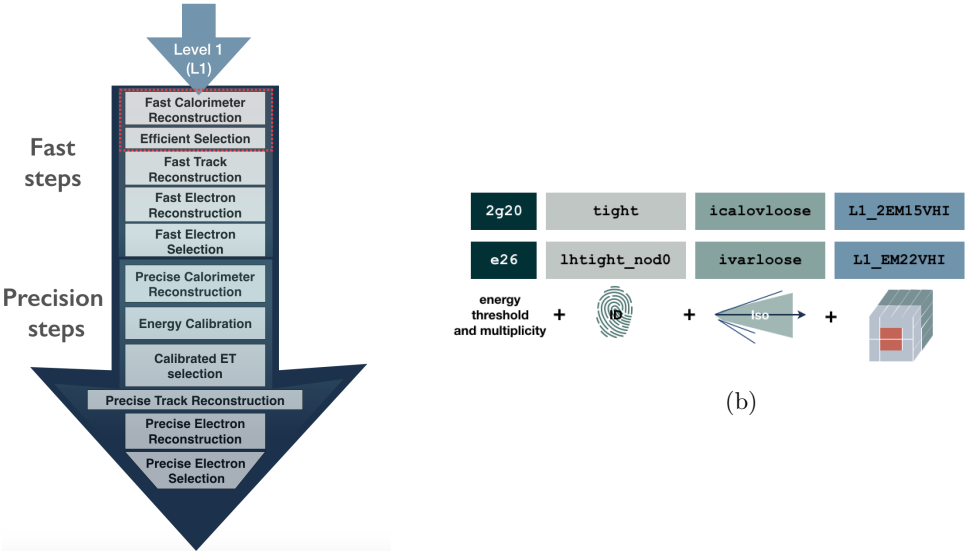

Fig. 2. The HLT algorithms run for an electron trigger (a), as well as the nomenclature for electron and photon triggers at the HLT (b), consisting of an energy threshold, an identification and (possible) isolation requirement, followed by the initial L1 trigger threshold.

(see the first two algorithms in Fig. 2(a)). A detailed explanation can be found in Ref. 3, here only the main principle will be sketched. The Ringer algorithm is applied for electrons with transverse energy, $E_{\mathrm{T}} > 15$ GeV. In each of the electromagnetic and hadronic calorimeter layers, a ring of calorimeter cells around the "hottest," most energetic cell is built. Normalised to the overall energy content in the region of interest, the ring energy sums are fed into a multilayer perceptron neural network. This procedure increases the processing time at the fast calorimeter step, but reduces the input candidates to the further tracking steps and therefore reduces the CPU demand significantly (around 50% for the lowest threshold, unprescaled single electron trigger).

3. Offline Processing

Once events have been selected by the L1 trigger and passed the HLT selection, those events are written on tape and can be further processed offline. This offline processing includes reconstruction, identification and possible checks on the isolation of the particles. The precision algorithms at the HLT are very close to those offline selections, with a few changes due to CPU restrictions. In this section, a brief overview of the offline processing, with a focus on its differences to the "online" reconstruction at trigger level is given, where a more detailed explanation can be found in Ref. 3.

Electrons at the HLT as well as offline are identified using a likelihood discriminator. There are three different working points of this likelihood discriminator: *loose*, *medium* and *tight*. In offline reconstruction, the Gaussian-Sum Filter (GSF) is used as a generalisation of the Kalman particle track fitter, better accounting for energy losses in the Inner Detector.[4] Due to CPU constraints, GSF was not used online. The offline photon identification is based on calorimeter variables, with two available working points, *loose* and *tight*, where *loose* relies on shower shapes in the second electromagnetic calorimeter layer and hadronic deposits. The *tight* working point additionally includes information from the first layer of the electromagnetic calorimeter, which has finer granularity information available.

A significant difference between offline and trigger reconstruction for electrons and photons is the usage of topological cell clusters, called superclusters, not used online. Those variable-sized clusters are used to adapt for possible Bremsstrahlung or pair production in the calorimeters, leading to close by electrons and photons, as detailed in Ref. 5.

4. Methods

Monitoring and measuring the rate and efficiency of electron and photon triggers is an important prerequisite to many physics analyses in ATLAS. To calculate the trigger efficiencies for electrons, a Z tag-and-probe method is used, whereas for photon trigger efficiencies a radiative Z decay or Bootstrap method is used. The details of this methods as well as the methodology of trigger rate measurements can be found in Ref. 3 and will not be discussed here.

5. Results

5.1. *Level-*1 *trigger performance*

Electron and photon High Level trigger are based on the same group of L1 trigger, selecting electromagnetic calorimeter clusters above certain energy thresholds. In Fig. 3, the L1 trigger rate is shown as a function of the instantaneous luminosity. By introducing a L1 isolation on the electromagnetic clusters (**I**) while keeping the same energy threshold, the trigger rate is reduced by up to 44% (see Fig. 3), while the efficiency drops by up to 5%. Compared to this, raising the energy threshold by 2 GeV (including a L1 isolation in both cases) decreases the rate by around 25% while the efficiency reduction is below 2%. This can be seen in Fig. 4(a) and 4(b), dependent on the transverse energy, E_{T} and the average number of interactions per bunch crossing, $\langle\mu\rangle$, also called pile-up.[3] Despite its efficiency reduction, introducing an additional L1 isolation has often been used in the adaption of the triggers during Run 2 to reduce trigger rates without increasing their thresholds.

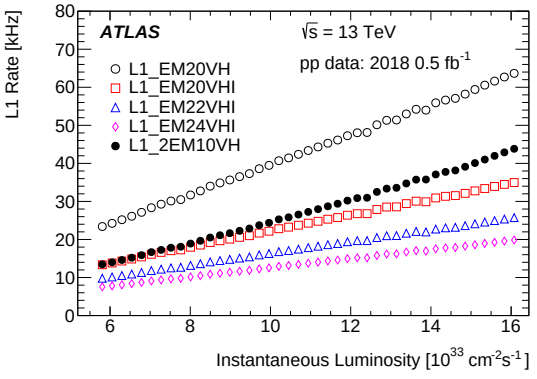

Fig. 3. Level-1 trigger rate in dependency of the instantaneous luminosity in a subset of 2018 data,[3] © ATLAS Collaboration.

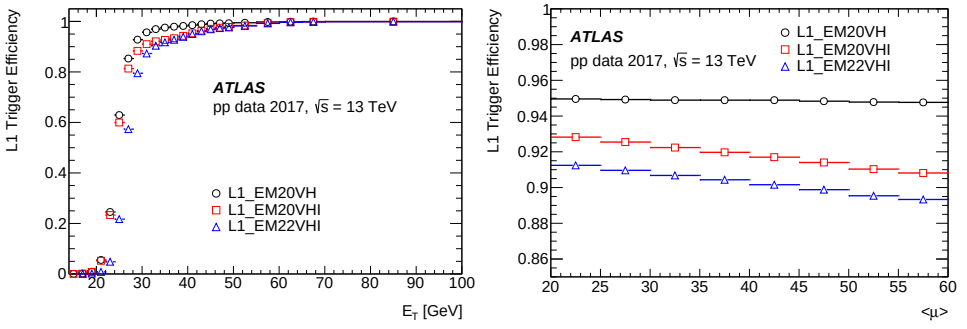

(a) (b)

Fig. 4. Level-1 trigger efficiency in dependency of E_{T} (a) and $\langle\mu\rangle$ (b), from Ref. 3, © ATLAS Collaboration.

5.2. *Photon trigger performance*

During Run 2, the lowest energy threshold single and diphoton triggers were adapted to the changing run conditions over the four years of LHC beam data, see Fig. 5(a) for single photon triggers and 5(b) for diphoton triggers. This was done in three different ways, increasing the energy threshold, increasing the identification requirement or introducing an isolation requirement, as can be seen in Table 1. After 2015, the single photon trigger energy threshold was raised by 20 GeV to keep the trigger rate below 50 Hz. Similarly in 2017, the rate of the primary diphoton trigger (which is mainly used by Higgs to diphoton analyses) was reduced by tightening the photon identification.

In Fig. 6, the single photon trigger efficiency is shown. A typical trigger "turn-on" curve can be seen, with a turn-on region close to the trigger threshold, where the trigger gains in efficiency, followed by a plateau region, in which the trigger efficiency stabilises and reaches its maximum value. For the single photon trigger,

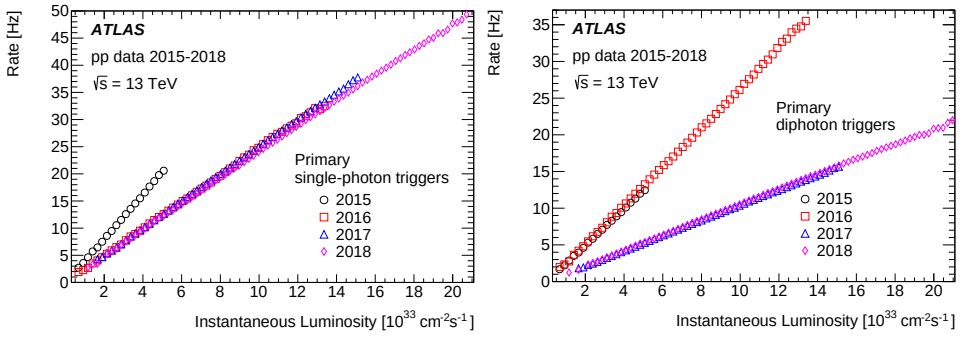

(a) (b)

Fig. 5. High Level Trigger Rate evolution in Run 2 for the primary single photon triggers (a) as well as the primary diphoton trigger (b),[3] © ATLAS Collaboration.

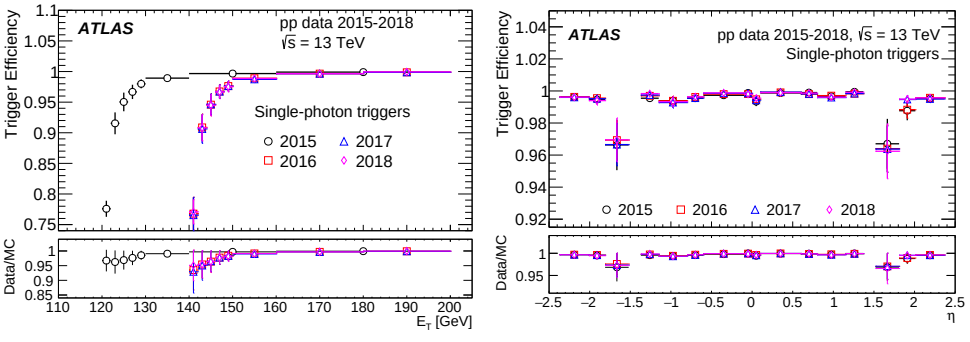

(a) (b)

Fig. 6. Efficiency of the single photon triggers from 2015 to 2018, in dependency of the transverse energy, E_{T} (a) and pseudorapidity, η (b), from Ref. 3, © ATLAS Collaboration.

a clear increase of the turn-on curves to higher E_{T} can be seen for data collected starting in 2016 (see Table 1). In 2016, the efficiency in the turn-on region rises minimally faster, which was due to lower pile-up conditions in 2016 compared to 2017 and 2018. The total uncertainties here are dominated by systematics, in the order of a few percent. The pseudorapidity dependency is flat apart from the η range close to the transition region of the barrel to the end-cap of the calorimeters.

Table 1. Evolution of the main lowest threshold photon trigger during Run 2.

	2015	2016	2017	2018
Single photon	`g120_loose`	`g140_loose`		
Primary diphoton	`g35_loose_g25_loose`		`g35_medium_g25_medium`	
Tight diphoton	`2g20_tight`	`2g22_tight`	2g20_tight_icalovloose	

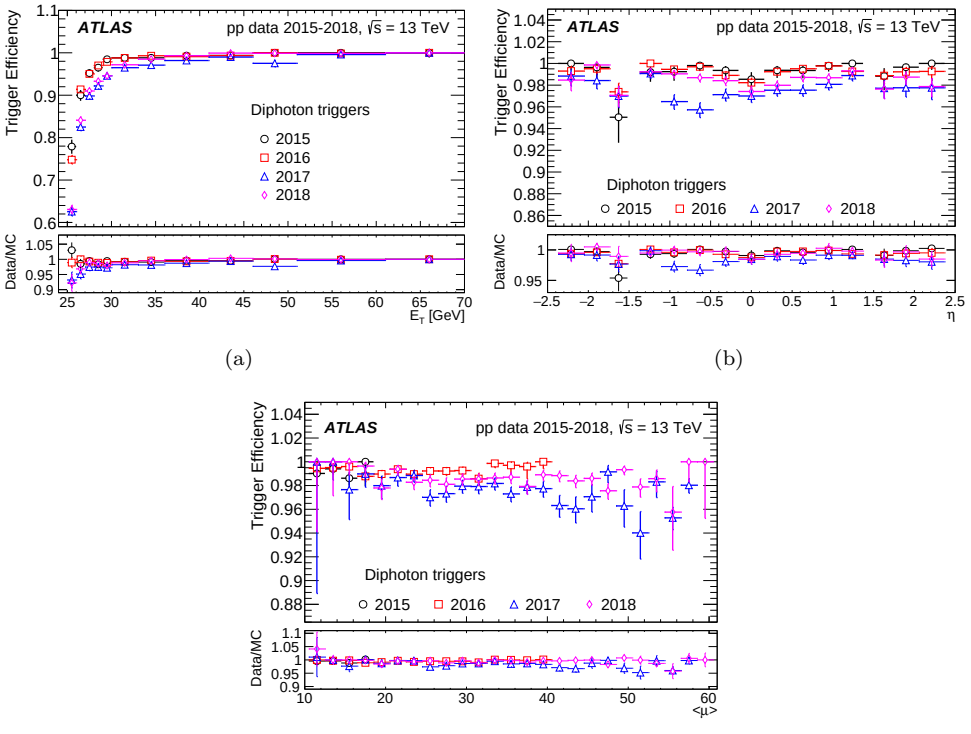

(a) (b)

(c)

Fig. 7. Efficiency of the diphoton trigger, illustrated by the 25 GeV photon part of the overall diphoton trigger. Given is the efficiency in dependency of E_{T} (a), η (b) and $\langle\mu\rangle$ (c), taken from Ref. 3, © ATLAS Collaboration.

For multi-object trigger, the trigger efficiency of each trigger leg is calculated separately and later on combined in the analyses. In Fig. 7, the 25 GeV photon part of the diphoton trigger efficiency, as calculated by the radiative Z decay method is shown. A small drop in efficiency can be observed moving from 2016 to 2017, which was due to tightening the identification criteria from *loose* to *medium*, as can be seen in Table 1. A different proton bunch structures in 2017 compared to 2018 leads to an increase in out of time pileup, which influenced the performance of shower shape variables in the photon trigger reconstruction. This is likely to be the explanation of the observed inefficiencies in 2017 diphoton triggers compared to their performance in 2018.

5.3. *Electron trigger performance*

The Ringer algorithm was introduced in 2017 as one of the main improvements in the electron trigger. During the commissioning and testing phase, dedicated triggers with and without the Ringer algorithm were run. The trigger efficiency increased slightly when adding the Ringer algorithm, as can be seen in Fig. 8. More importantly the CPU usage was reduced by around 50%.

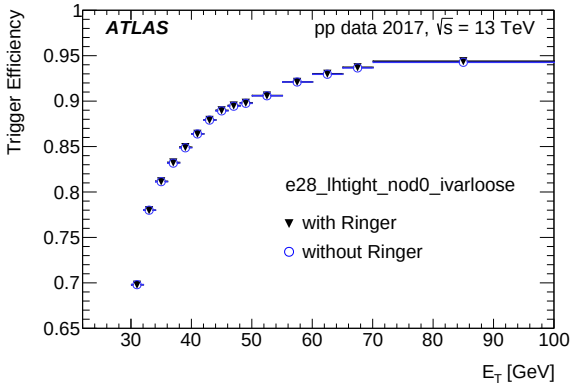

Fig. 8. Performance of the 28 GeV electron trigger with the Ringer algorithm or the "Fast Calorimeter" reconstruction without the Ringer algorithm (based on calorimeter variables) in 2017,[3] © ATLAS Collaboration.

Table 2. Evolution of the unprescaled electron triggers during Run 2.

	2015	2016	2017	2018

Single electron	`e24_lhmedium (EM20VH)`
	`e120_lhloose`
	`e200_etcut`
		`e26_lhtight_nod0_ivarloose` (EM22VHI)
		e60_lhmedium_nod0
		e140_lhloose_nod0
		e300_etcut		

Di-electron	`2e12_lhloose (2EM10VH)`	`2e17_lhvloose_nod0 (2EM15VH)`	`2e17_lhvloose_nod0 (2EM15VHI)` `2e24_lhvloose_nod0 (2EM20VH)`	

In Table 2, the evolution of the single electron as well as double electron trigger with the lowest unprescaled energy thresholds can be seen. As shown in Fig. 9, the trigger rate for 2015 increased significantly with the rising instantaneous luminosity, so that from 2016 on not only the threshold but also the trigger identification had to be raised, as well as an isolation introduced. The single electron trigger is constructed as a logical OR between multiple, increasing threshold triggers. As the threshold, the identification and isolation criteria can be loosened, which reaches a higher trigger efficiency.

The step-like behavior especially around 60 GeV in the switch between the lowest threshold trigger with *tight* identification to a higher threshold with only *medium* identification criteria can be seen in Fig. 10. In the E_{T} dependence, an earlier turn on of the 2015 efficiency can be observed, based on its lower threshold compared to the following years. Even though the trigger is identical from 2016 to 2018, several changes in the underlying algorithms have led to varying efficiencies. Just to mention one influencing factor, in 2015 and 2016 the precision calorimeter reconstruction was based on a likelihood method, whereas in the following years this was solely based on E_{T} cuts. Further changes in the algorithms can be found in Ref. 3.

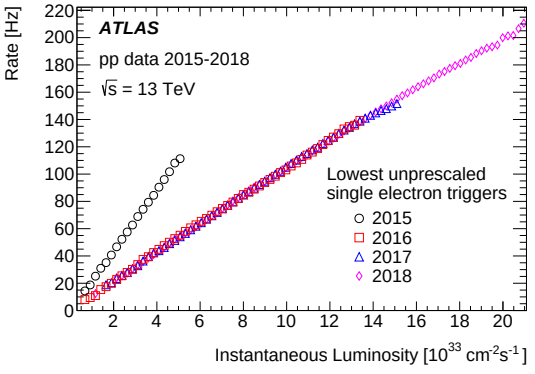

Fig. 9. Evolution of the unprescaled electron triggers during Run 2,[3] © ATLAS Collaboration.

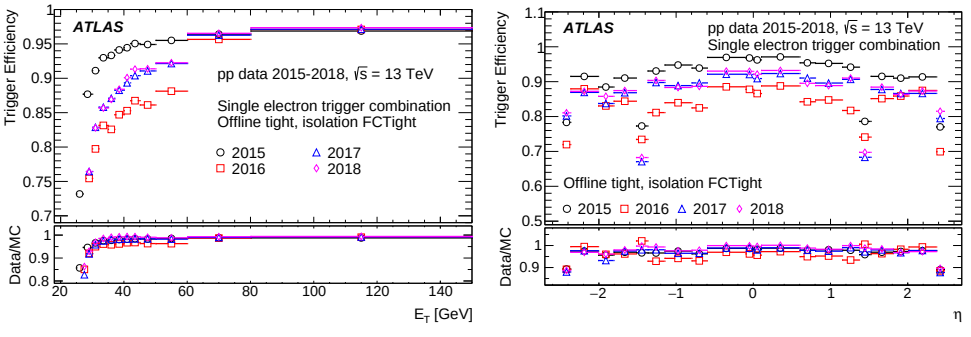

(a) (b)

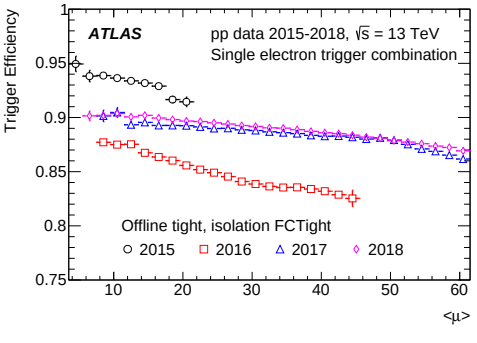

(c)

Fig. 10. Single electron trigger efficiency in terms of E_{T} (a), η (b) and $\langle\mu\rangle$ (c),[3] © ATLAS Collaboration.

6. Conclusions

In this paper, an overview of the performance of electron and photon triggers in the ATLAS experiment during Run 2 of the Large Hadron Collider has been presented. Several methods have been used during Run 2 to study and compare the efficiency

performance of electron and photon triggers. In this summary, only the behavior of single electron (photon) as well as diphoton triggers have been discussed, with those triggers being used by many physics analyses in ATLAS.

References

1. ATLAS Collab., *J. Instrum.* **3**, S08003 (2008).
2. J. Wenninger, Operation and configuration of the LHC in Run 2, https://cds.cern.ch/record/2668326.
3. ATLAS Collab. Performance of electron and photon triggers in ATLAS during LHC Run 2, arXiv:1909.00761.
4. T. Atkinson, Reconstruction of electrons with the Gaussian-Sum Filter in the ATLAS inner detector, doi:10.1109/NSSMIC.2005.1596226.
5. ATLAS Collab., Electron and photon reconstruction and performance in ATLAS using a dynamical, topological cell clustering-based approach, ATL-PHYS-PUB-2017-022, https://cds.cern.ch/record/2298955.